8th Biennial International Conference
& Exposition on Petroleum Geophysics

"HYDERABAD 2010"

P-246

Interpreting CSEM data in complex resistivity regime

Lars Lorenz* and Håkon Pedersen, *EMGS ASA,*
Muralikrishna Akella, Anil Tyagi, Pranaya Sangvai and Rabi Bastia, *Reliance Industries Ltd.*

Summary

Controlled Source Electromagnetics (CSEM) provides a powerful tool for the risk mitigation process. This study gives a case example for the application of CSEM to reduce risks in drilling decisions. It underlines the importance of using all available resistivity information in the form of well logs as well as existing CSEM data in the integration, including the interpretation of the inversion results. A discussion of the integration is performed, taking into account the uncertainties in the assumptions for different parts of the subsurface, and shows how the ranking of the prospects, based on CSEM data, is interwoven with the perceived uncertainties. Drilling results yielded a commercial hydrocarbon discovery for one of the highest-ranked targets.

Introduction

Exploration in the Krishna-Godavari (KG) Basin at the East Coast of India by Reliance and other oil companies yielded several world-class oil and gas discoveries. The basin is characterized by a wide range of depositional settings, ranging from coastal plains, deltas and shelf-slope aprons to deep-sea fans. Commercial accumulations of hydrocarbons occur in sediments of Permian to Pliocene age. The most significant hydrocarbon potential, and currently targeted prospective play type, can be found in the tertiary channel–levee–overbank sediments of Mio- to Pliocene age in deep waters.

Reliance has large acreage in the KG Basin with most areas in water depths beyond 200 m. This required mitigating the risk before drilling due to the significant associated costs. For this purpose, Reliance employed CSEM to identify high-resistive thin beds, a common characteristic of hydrocarbon reservoirs. Successful CSEM application to targets in the Pleistocene and Pliocene interval (Tyagi et al., 2008) and refinement of the resistivity information for the area based on the interpretation of the existing CSEM data, encouraged targeting of deeper intervals in the area as well.

Method

A detailed description of the CSEM technique is provided by Eidesmo et al. (2002) and Ellingsrud et al. (2002). A low frequency electromagnetic signal is emitted by a horizontal electric dipole into the seabed and underlying sediments. The electromagnetic field diffuses through the sediment column and is rapidly attenuated due to low resistivitiy of saline pore fluids. If the field encounters a high-resistive layer and enters it at a critical angle of incidence, the energy is guided along the layer with a significantly smaller degree of attenuation and is constantly refracted back to the seafloor where it is recorded by electromagnetic receivers (Kong et al., 2002). The detection of this guided and refracted energy is the basis of CSEM (Ellingsrud et al., 2001).

Background Information for the Survey Area

The prospects in the survey area are characterized by a wide range of burial depths, ranging from targets in the Late Pliocene to the Early Miocene (Figure 1). Wells drilled in the channel-levee complex of the Pleisto-Pliocene section encountered reservoir sands with thicknesses varying from few millimeters to 60 m. Depending on reservoir thickness, the reservoir resistivities were highly variable as well.

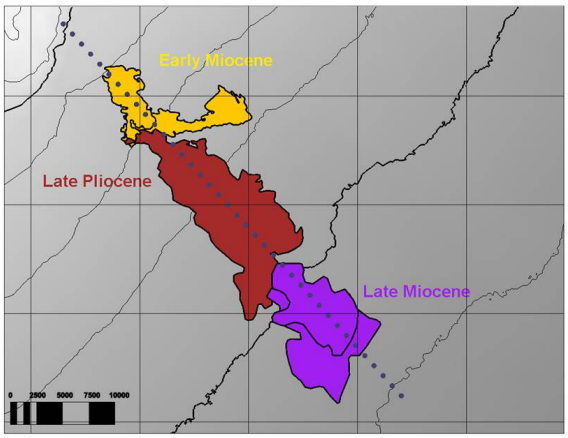

Figure 1: Survey Map with prospect polygons at different stratigraphic intervals. Prospect polygons in color, receiver positions as grey circles.

The shale resistivity as measured by the standard logging suite is normally around 0.7-0.9 ohmm. Interpretation of previously collected CSEM data in the Krishna-Godavari Basin (Tyagi et al., 2008, Suffert et al., 2008), as well as available anisotropy logs indicated a higher vertical resistivity, about 1.5 to 2.0 times higher than the horizontal resistivity.

While the higher background resistivity improved the ability to inject currents in the deeper section of the subsurface due to lower attenuation, it helped in a very limited manner to address the high variability of the reservoir resistivities which even for the vertical resistivity as measured by anisotropy logs could be as low as 5 ohmm. Therefore, a careful assessment of the survey parameters had to be performed.

Pre-survey modeling and survey parameters

Pre-survey modeling was performed for the diverse prospects to evaluate the sensitivity of CSEM in the different target intervals. Uncertainties existed for the background resistivity of the deeper Miocene interval. Even though CSEM measurements for calibrating the resistivity of this interval were in principle available through other surveys in the area, there were uncertainties regarding how representative those measurements were.

It was therefore decided to extrapolate the Pliocene resistivities to the deeper section. Even though not ideal, 1D modeling suggested that this was a pessimistic assumption. While the predicted response for the higher resistive Early Miocene reservoirs was not strongly affected by the slightly lower resistivity contrast, the frequency range with sensitivity to these deeper targets was significantly lower.

The following 3D feasibility study suggested that detectable responses could be recorded from the different targets. On the other hand, the frequencies with the highest sensitivity were spread out widely across the frequency band due to the different target depths (Figure 2). It was therefore decided to acquire the survey by two source tows with two frequency spectrums to allow for a large enough frequency range with sensitivity to the targets for reliable inversion results.

A receiver spacing with 1.25 km was chosen to ensure sufficient data coverage for follow-up inversion of the data, and the survey line placed as centrally as possible over all the prospects, as this yielded the highest response in the pre-survey modeling (Figure 1).

Data Interpretation

The interpretation was performed in three stages. An initial assessment of the relative response variation was followed by an unconstrained Inversion and concluded by a 3D modeling study.

Utilizing relative responses by using normalized magnitude (NMvO) and phase difference (PDvO) indicated the presence of local resistive features in the shallow and deep sections of the subsurface. A significant increase in the complexity of the resistivity regime in the deeper section towards larger water depths was observed as well. Figure 3 illustrates this, comparing the response of short source-receiver offsets and high frequency, probing the shallow subsurface, and the response of large source-receiver offset and low frequency, probing a much deeper interval.

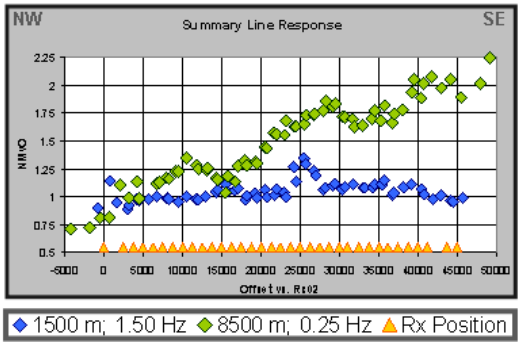

Figure 3:NMvO and PDvO responses at high frequency – low offset and large offset – low frequency, illustrating presence of local resistors as well as increasing complexity with depth.

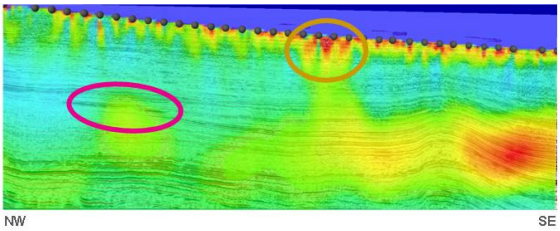

Figure 4: 3D inversion result with a half-space starting model. Higher resistive local events marked by colored circles.

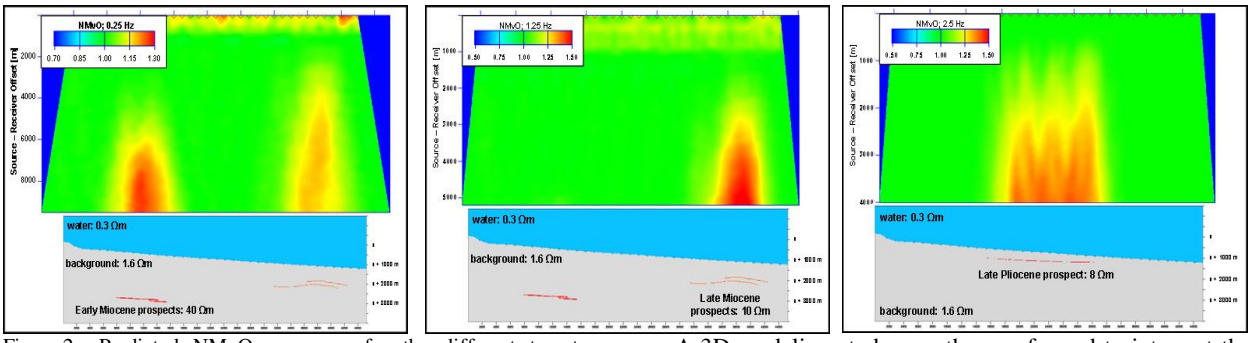

Figure 2: Predicted NMvO responses for the different target intervals at the frequencies with highest sensitivity to the respective target. Only data above the anticipated noise floor is presented. Models for the respective targets are presented together with the response.

To improve the precision for the depth allocation of the resistive events and to transfer the analysis from a qualitative to a quantitative level, an unconstrained inversion was performed. A 3D inversion scheme as described by Zach et al. (2008) was utilized for the unconstrained inversion.

The unconstrained 3D inversion result with a half-space starting model is shown in Figure 4. Two defined local resistive events occur, a shallow event in the Late Pliocene (brown), and a deeper event in the Early Miocene (red). Both events correlate well with indicated prospects. Additionally, higher resistivities in the Early- to Mid-Miocene are present in the SE part of the line.

A 3D modeling study was then performed to interpret the unconstrained inversion results. With the limited number of calibration areas for the 3D model, it was decided to keep the background model as simple as possible and as high resistive as possible. This approach was motivated by the intention to retrieve the most robust anomalies, yielding the highest confidence and thereby allowing to high rank these targets.

The resulting background model in Figure 5 is very close to a half space. The incorporated resistivities are at the upper end of the measured vertical resistivity values, increasing the confidence that it is more likely that too much of the response was attributed to the background resistivity than too less.

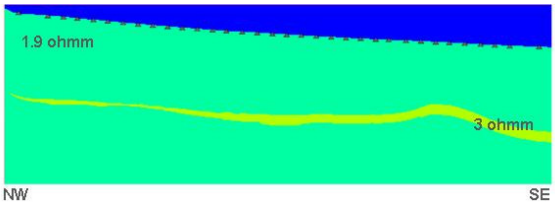

Figure 5: Derived background model with most simplified geometry and highest resistivity

The remaining data misfit between the synthetic model and the real data was then addressed through incorporation of thin resistors. First, the reservoir type resistors were introduced in the shallow section. After no further improvements in data fit could be obtained by variations of the shallow resistor properties, deeper resistors were introduced to improve the remaining data misfit (Figure 6). This strategy yielded a very low data misfit (Figure 7).

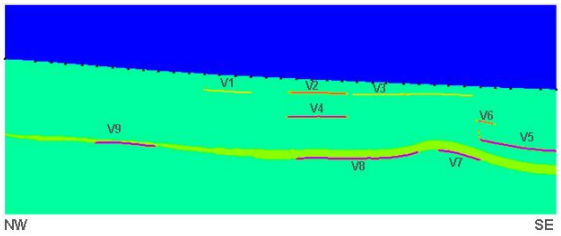

Figure 6: Resulting model with all introduced reservoir type resistors for best achievable data misfit, based on background model in Figure 5.

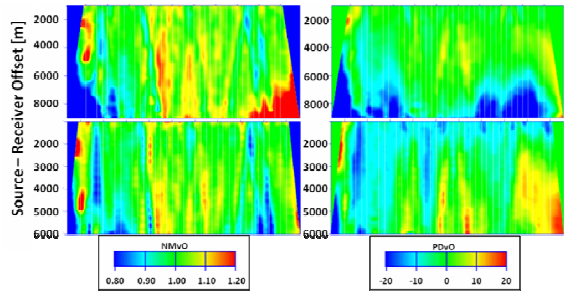

Figure 7: Data misfit between real data and synthetic data of reservoir type resistor model in Figure 6 for magnitude and phase at two different frequencies.

Nevertheless, a varying degree of confidence existed for the various resistors. V1 to V3 were attributed a high degree of confidence due to their shallow position and resulting limitations in possible background variations. In the deeper section, V9 was a very consistent stand alone event for relative response as well as inversion results, therefore considered as a high confidence target as well. For the additional deeper targets, alternative scenarios with higher complexity for the background configuration would yield anti-models to the reservoir type resistor scenario.

Following the initial CSEM interpretation, it was recommended to drill the high confidence targets first and to re-interpret the data set after well log information is available as additional calibration data for the model. The presence of hydrocarbons in the Early Miocene target V9 was confirmed by the subsequent drilling (Figure 8).

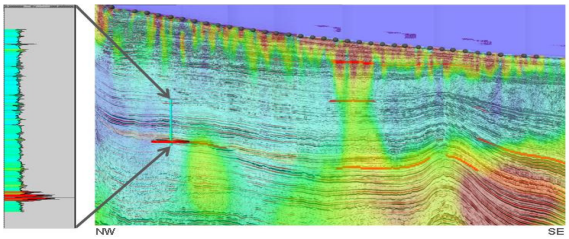

Figure 8: Seismic cross section with indicated well log, overlain by unconstrained 3D inversion result and 3D modeling result.

Post Drilling Analysis

Using the well log as a new calibration point, a post drilling analysis was performed. This analysis aimed on increasing the confidence in the presence of the additional Early- and Mid Miocene resistors for a more complex subsurface resistivity model. The complexity of the subsurface was increased by introducing a more detailed subsurface structure. Anisotropy was neglected as a 3D modeling check indicated minor deviations between an anisotropic model and an isotropic, vertical resistivity based model for the 2D deep water data as present here.

Even though additional calibration information was present, significant gaps in the resistivity knowledge of the subsurface remained. Therefore, various hypotheses for the link between subsurface structure and resistivity were tested. For this purpose, a 2.5D inversion scheme was utilized and the various resistivity – structure links introduced in form of constrains. Figure 9 shows some of the results of the constrained 2.5D inversion as well as an unconstrained 2.5D inversion result as a reference.

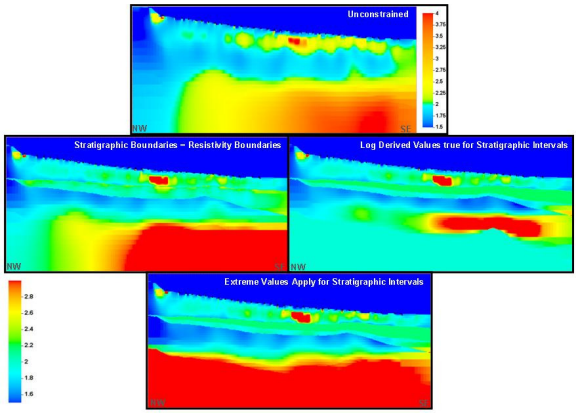

Figure 9: Unconstrained 2.5D inversion result (top) and various constrained inversion results (middle and bottom). Premise for constrains are given in figure text.

All constrained inversion results have in common the occurrence of higher resistivities in the Mid-Miocene section. This is even the case for the inversion runs where it was attempted to allocate all the higher resistivities to the Early Miocene interval by locking the resistivities at the absolute maximum value derived, nearly twice the value indicated by the well logs (Figure 10). This significantly increased the confidence that the higher resistivities cannot be explained by a higher complexity of the model. A localized form of resistivity increase, e.g. a reservoir or tight formation, is required.

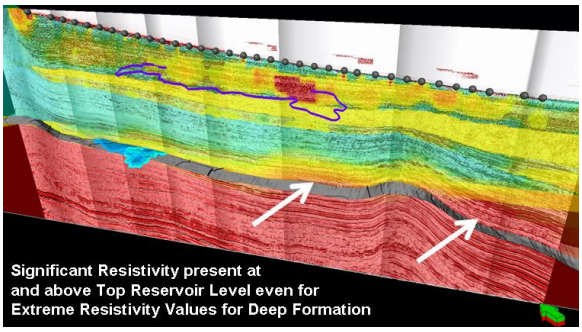

Figure 10: Early Miocene maximum resistivity constrained inversion result versus seismic, indicating requirement for localized resistivity increase.

Discussion and Results

We presented an interpretation work flow for a CSEM data set. Significant complexity of the response and limitations in the available calibration areas did not allow confidently interpreting the full data set in the first pass. This resulted in a simplified interpretation approach, characterized by the motivation to err at the side of caution.

Numerous possible targets were identified, and the high confidence targets, least affected by the simplifications in the interpretation approach, prioritized for drilling. Drilling results for one of the targets confirmed the presence of hydrocarbons. The following re-interpretation confirmed the requirement for at least some of the additional local resistors. This motivated the client to allocate the resources for a review of the geological model and the seismic to upgrade the CSEM identified leads to prospects.

References

Eidesmo, T., Ellingsrud, S., MacGregor, L.M., Constable, S., Sinha, M.C., Johansen, S., Kong, F.N. & Westerdahl, H. [2002] Sea Bed Logging (SBL), a new method for remote and direct identification of hydrocarbon filled layers in deepwater areas, *First Break*, 20, March, 144 – 152

Ellingsrud, S., Sinha, M.C., Constable, S., MacGregor, L.M., Eidesmo, T. & Johansen, S. [2002] Remote sensing of hydrocarbon layers by Sea Bed Logging (SBL): results from a cruise offshore Angola, *The Leading Edge*, **21**, 972 – 982

Johansen, S.E., Amundsen, H.E.F and Wicklund, T.A. (2007) Interpretation example of marine CSEM data. *The Leading Edge, Volume 26, Issue 3, pp. 348-354*

Kong, F.N., Westerdahl, H., Ellingsrud, S., Eidesmo, T. & Johansen, S. (2002) Seabed logging: A possible direct hydrocarbon indicator for deepsea prospects using EM energy. *Oil & Gas Journal,* May 13

Mittet, R. and Schaug-Pettersen, T. (2007) Shaping optimal transmitter waveforms for marine CSEM surveys, *SEG Technical Program Expanded Abstracts 2007*, pp. 539-543

Mittet, R., Maaø, F.A., Aakervik, O.M., and Ellingsrud, S. (2005) A two-step approach to depth migration of low frequency electromagnetic data, *SEG Technical Program Expanded Abstracts 2005*, pp. 522-525

Maaø, F.A. (2007) Fast finite-difference time-domain modeling for marine-subsurface electromagnetic problems, *Geophysics 72*, pp. A19-A23

Zach et al., SEG 2008 Extended Abstract "3D inversion of marine CSEM data using a fast finite-difference time-domain forward code and approximate Hessian-based optimization"

Støren T., Zach J.J., Maaø, F.A. (2008) Gradient Calculations for 3D Inversion of CSEM Data Using a Fast Finite-difference Time-domain Modelling Code, EAGE Technical Program Extended Abstract

Tyagi et al.

Suffert et al.